JOURNAL OF MATERIALS SCIENCE **40** (2005) 1353– 1357

Counterion effects in cyanine heterojunction photovoltaic devices

F. NÜESCH*
EMPA, Materials Science and Technology, Überlandstrasse 129, CH-8600 Dübendorf, Switzerland; Laboratoire d'optoélectronique des matériaux moléculaires, Institut des matériaux, EPFL, CH-1015 Lausanne, Switzerland
E-mail: frank.nueesch@empa.ch

A. FAES, L. ZUPPIROLI
Laboratoire d'optoélectronique des matériaux moléculaires, Institut des matériaux, EPFL, CH-1015 Lausanne, Switzerland

FANSHUN MENG, KONGCHANG CHEN, HE TIAN
Institute of Fine Chemicals, East China University of Science & Technology, Shanghai 200237, People's Republic of China

We investigated cyanine heterojunction photovoltaic devices using carbocyanine dyes as donors and buckminsterfullerene (C60) as acceptor. In particular, we focused on the influence of cyanine counterions on the photovoltaic device characteristics. It was found that counterions can be displaced in the applied electric field and give rise to important hystereses in the current-voltage characteristics, which are related to charge injection processes at electrode and organic heterointerfaces. Mobile counterions have also a drastic effect on the photocurrent spectrum and are responsible for an important C60 contribution at the organic heterojunction between cyanine and C60. If the counterion is covalently linked to the cyanine dye, the C60 contribution in the blue spectral domain can not be observed.

1. Introduction

Organic photovoltaics is a promising technology for low cost solar energy conversion, in particular when the materials involved in device fabrication benefit from solution processing. Since the discovery of ultrafast photoinduced electron transfer from conjugated polymers to buckminsterfullerene (C60) [1] and the introduction of the "bulk heterojunction" concept [2], the efficiency of polymer photovoltaic devices has been improved steadily in recent years [3–7].

The most popular material classes used in polymer donor-acceptor heterojunction solar cells are among the poly(para-phenylenevinylenes) [8], poly(thiophenes) [9] and poly(fluorenes) [10] and are usually electrically neutral compounds.

Cyanine dyes have been studied for decades for their application in silver halide photography [11]. Several requirements that are important to classical photography are also crucial to organic solar cells. Particularly interesting are the high extinction coefficients, tunable absorption spectra and the possibility to form aggregates. Furthermore, the energy levels of the cyanine frontier orbitals are such that they can be used as donors and acceptors in heterojunction photovoltaic devices [12]. Unlike other small conjugated molecules used in organic photovoltaics [13–15], cyanine dyes can be easily spin-coated from solution, which is of considerable technological interest. Additionally, cyanines are cationic dyes, meaning that they are always accompanied by negative counterions. While the effect of counterions on the photophysical properties of cyanine dyes has been addressed in solution [16] and at oxide surfaces [17], ion effects in solid organic photovoltaic devices have received little attention.

In this work, we have investigated counterion effects on the photoelectrical characteristics of heterojunction devices based on cyanine dyes and C60. For this purpose, two cyanine dyes with identical chromophores were synthesized, where one compound has a covalently linked counterion, while the other owes a free counterion.

2. Experimental

The chemical structures of the materials used in this study are shown in Fig. 1. Poly(3,4-ethylenedioxythiophene) poly(styrenesulfonate) (PEDOT:PSS) (Baytron) was supplied by Bayer and was filtered using successive filter pore sizes of 5, 1.2 and 0.8 μm. C60 (purified) was supplied by SES Research

*Author to whom all correspondence should be addressed.

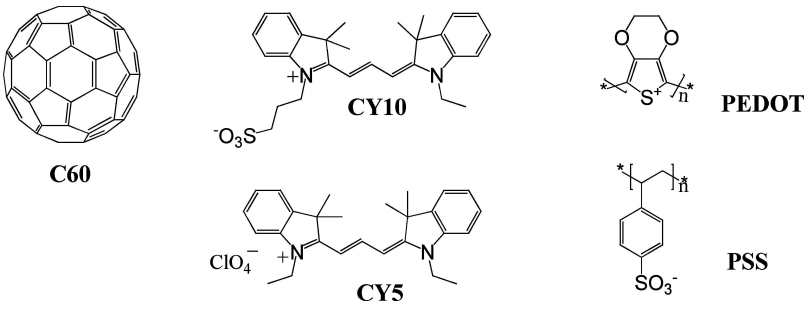

Figure 1 The chemical structures of the materials used in this study.

Inc.1,1′-diethyl-3,3,3′,3′-tetramethylcarbocyanine perchlorate (CY-5) and 1-sulfopropyl-1′-ethyl-3,3,3′,3′-tetramethylcarbocyanine (CY-10) were synthesized in our laboratory based on published procedures [18, 19].

Synthesis of 2-[3-(1,3-dihydro-3,3-dimethyl-1-ethyl -2H-indol-2-ylidene)-propenyl]-3,3-dimethyl-1-sulfopropyl-3H-indolium inner salt: A mixture of 1-sulfopropyl-2,3,3-trimethyl-3H-indolium inner salt (2.81 g, 10 mmol), 2-(1-ethyl-3,3-dimethylindolin-2-ylidene)acetaldehyde (2.14 g, 10 mmol) and acetic anhydride (30 mL) was heated for 1 h at 100∼110°C. The reaction mixture was poured into water (150 mL) and stirred at room temperature overnight. The aqueous solution was extracted with dichloromethane and the dichloromethane solution was washed three times with water. The dichloromethane solution was dried over $MgSO_4$ and evaporated under vacuum. Then, the residue was purified by column chromotagraphy (silica gel, dichloromethane/methanol 20:1) to afford 3.8 g (80%) solid.

^{1}H-NMR (DMSO-d_6, 500 MHz): δ 1.31 (*t*, 3H, $-CH_2CH_3$), 1.67–1.69 (*d*, 12H, $-C(CH_3)_2$, $-C(CH_3)_2$), 2.05 (m, 2H, $-CH_2CH_2CH_2-$), 2.56 (*t*, 2H, $-CH_2CH_2CH_2-$), 4.16 (*m*, 2H, $-CH_2CH_3$), 4.26 (*t*, 2H, $-CH_2CH_2CH_2-$), 6.49 (*d*, 1H, $J = 13.43$ Hz, $-CH=CH-CH=$), 6.62 (*d*, 1H, $J = 13.46$ Hz, $-CH=CH-CH=$), 7.29 (*t*, 2H, Ar–H), 7.42–7.47 (*m*, 3H, Ar–H), 7.56 (*d*, 1H, $J = 7.97$ Hz, Ar–H), 7.63 (*d*, 2H, $J = 7.42$ Hz, Ar–H), 8.34 (*t*, 1H, $-CH=CH-CH=$). Anal. Calcd. for $C_{28}H_{34}N_2O_3S$: C 70.26, H 7.16, N 5.85%. Found: C 70.14, H 7.19, N 5.90%.

Synthesis of 2-[3-(1,3-dihydro-3,3-dimethyl-1-ethyl-2H-indol-2-ylidene)-propenyl]-3,3-dimethyl-1-ethyl-3H-indolium perchlorate: A mixture of 1-ethyl-2,3,3-trimethyl-3H-indolium iodide (5.62 g, 20 mmol), triethyl orthoformate (1.48 g, 10 mmol) and pyridine (50 mL) was refluxed for 5 h. The reaction mixture was poured into water (250 mL) and stirred at room temperature overnight. The solid was filtered and washed with water. The crude product was dissolved in ethanol at reflux temperature and 4.8 g sodium perchlorate hydrate was added. The solution was refluxed for 0.5 h and then cooled down overnight. The precipitated solid was recrystallized again from ethanol to give 3.2 g (67%) solid.

^{1}H-NMR (DMSO-d_6, 500 MHz): δ 1.33 (*t*, 6H, $-CH_2CH_3$), 1.70 (*s*, 12H, $-C(CH_3)_2$), 4.17 (*m*, 4H, $-CH_2CH_3$), 6.53 (*d*, 2H, $J = 13.45$ Hz, $-CH=CH-CH=$), 7.31 (m, 2H, Ar–H), 7.44–7.48 (*m*, 4H, Ar–H), 7.65 (*d*, 2H, $J = 7.44$ Hz, Ar–H), 8.36 (*t*, 1H, $-CH=CH-CH=$). Anal. Calcd. for $C_{27}H_{33}ClN_2O_4$: C 66.86, H 6.86, Cl, 7.31, N 5.78%. Found: C 66.93, H 6.74, N 5.83%.

Cyclic voltammetry measurements were recorded on an EG&G Versastat II potentiostat using a glassy carbon working electrode, a platinum counter-electrode and an Ag/AgCl reference electrode with a reference potential of 0.21 V vs. NHE. Concentrated dye solutions in dichloromethane (Fluka, puriss. over molecular sieve) containing 0.1 M tetrabutylammonium perchlorate were purged with nitrogen to avoid oxygen contamination. Typically, three cycles were performed before acquiring the data. The redox potentials E_{red} and E_{ox} related to the lowest unoccupied molecular orbital (LUMO) and highest occupied molecular orbital (HOMO), respectively, were determined by taking the middle value between the peaks of the oxidation and reduction wave. According to the calculation by Noyes [20], the NHE potential is taken to be −4.5 eV vs. vacuum. This leads to a potential of −4.71 eV vs. vacuum for the reference electrode used here. The respective frontier orbital energy levels obtained for cyanine dyes CY5 and CY10 are indicated in Fig. 2a together with the energy diagram of the devices used in this work. The frontier orbital energy levels of C60 and PEDOT:PSS were inferred from the literature [21, 22].

Multilayer photovoltaic devices (see Fig. 2b) were fabricated both by spin coating and thermal evaporation procedures on indium tin oxide (ITO, AFC) glass substrates with a sheet resistance of 30 Ohm/square. The ITO substrates were first cleaned in ethanol, acetone and soap ultrasonic bathes. Then, a 80 nm thin PEDOT:PSS layer was spin coated onto the conducting glass substrate. The coated substrates were subsequently transferred to a vacuum chamber where they

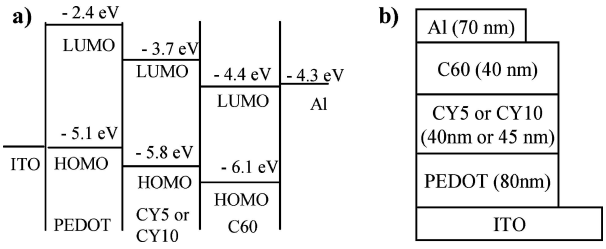

Figure 2 Energy level diagram (a) and corresponding device architecture (b). The HOMO and LUMO levels of cyanines CY5 and CY10 and the other materials are also indicated in the graph.

were heated under vacuum at 90°C for several hours. After the heating process the substrates were cooled to room temperature and spin coated with a thin cyanine layer of either CY5 or CY10. The thicknesses of CY5 and CY10 were 40 and 45 nm, respectively and were inferred from profilometry measurements on reference substrates using a Tencor Alpha-Step 500 profilometer. Then the substrate was conveyed to a vacuum chamber (base pressure $<10^{-6}$ Torr) where it was kept at 35°C for 12 h. A 40 nm thick C60 layer was then vapor deposited. Finally, an aluminum top electrode was vapor deposited through a shadow mask.

Photocurrent spectra were measured using monochromatic light from a JY HR 460 monochromator with a tungsten halogen lamp source. The intensity of the monochromatic light beam was measured using a Grasby Optronics 247 calibrated radiometric photodiode.

Current-voltage (I-V) characteristics were measured in nitrogen atmosphere using a Keithley 236 source-measure unit. A tungsten halogen lamp was used for white light irradiation from the ITO side. To vary the unfiltered irradiation intensity of 310 mW/cm^2, neutral density filters (ND1, ND2) were used.

Absorption spectra of thin film devices were measured using a Varian (Cary 50) Spectrophotometer.

3. Results and discussion

3.1. Current-voltage characteristics in the dark

Before measuring the photovoltaic characteristics of the devices, current-voltage curves were recorded to exclude short circuit problems. Fig. 3 shows typical dark current-voltage curves of heterojunction devices described in the previous section. Interestingly, there is a significant difference between devices using a cyanine layer with covalently linked counterions (Fig. 3a) and devices using a cyanine layer with free counterions (Fig. 3b). For the latter, the current density at reverse bias (negative bias applied to the ITO electrode) is much more important than the forward current density. Furthermore, clear hysteretic behavior can be observed, which is less important for devices using immobile counterions.

The hysteretic behavior depends on the sweep speed of the current-voltage scan and is a clear signature of slowly moving charges. Since the effect is only seen for cyanine layers having free counterions, we have attributed this behavior to the perchlorate counterions of CY5. Being displaced in the applied electric field, anions move towards the C60 layer, leaving positively charged cyanine molecules at the PEDOT interface. Similarly to an electrochemical device [23], positive charges facilitate electron injection from PEDOT giving rise to an important current density under reverse bias. At forward bias (positive bias applied to the ITO electrode) there is a considerable energy barrier to be crossed at the cyanine/C60 interface (see energy diagram in Fig. 2a). The current density is therefore not only limited by charge injection from both electrodes, but also by charge recombination at the organic heterointerface. Mobile ions can also modify the organic heterojunction barrier, which might explain the hysteretic behavior under forward bias.

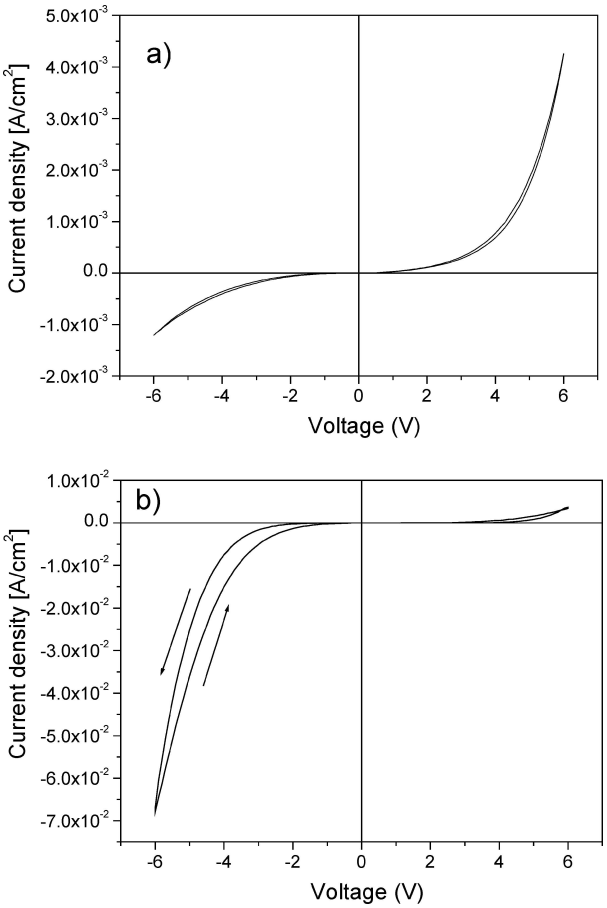

Figure 3 Dark current-voltage characteristics of a device based on CY10 with covalently linked counterions (a) and an analogue device based on CY5 with free counterions (b). The phase was connected to ITO.

3.2. Current-voltage under irradiation

The photocurrent obtained under illumination using a tungsten halogen lamp is shown is Fig. 4. The device with covalently linked counterions (Fig. 4a) has relatively small short-circuit photocurrents J_{sc}. The short circuit current increases linearly with irradiation intensity, indicating that there is no current saturation. The open circuit voltage V_{oc} increases with irradiation intensity and reaches up to 0.7 V at a white light intensity of 310 mW/cm^2. The fill factor FF represents the degree of ideality of the device and is defined as

$$FF = \frac{(J \cdot V)_{max}}{V_{oc} \cdot J_{sc}} \qquad (1)$$

where $(JV)_{max}$ is the maximum electrical power output of the device. FF decreases from 0.28 to 0.23 when increasing the irradiation intensity form 0.31 to 310 mW/cm^2. The power conversion efficiency η is calculated as:

$$\eta(\%) = \frac{FF \cdot V_{oc} \cdot J_{sc}}{P_{in}} \times 100\% \qquad (2)$$

where P_{in} is the incident light intensity. The power efficiency for devices with linked counterions is rather

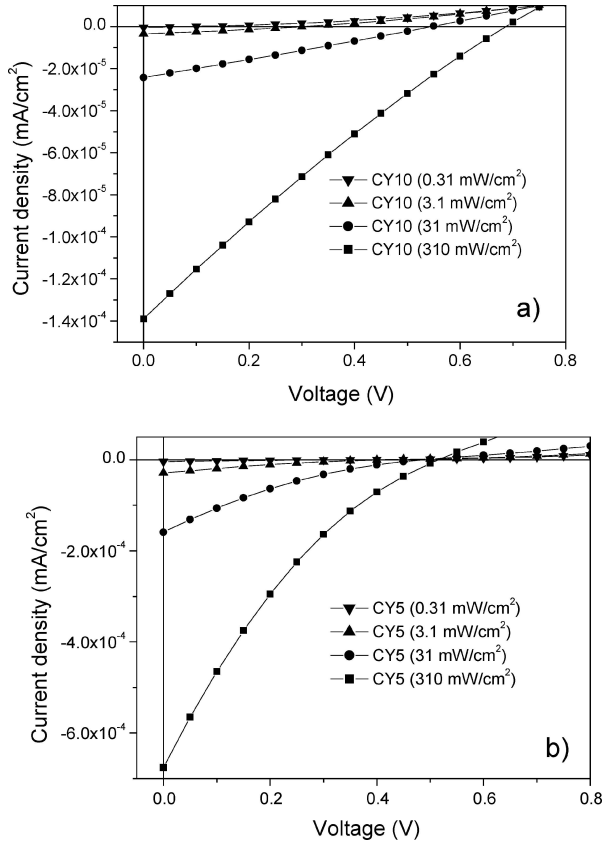

Figure 4 Current-voltage characteristics of devices based on CY10 with covalently linked counterions (a) and devices based on CY5 with free counterions (b). The irradiation intensities 310 mW/cm^2 (squares), 31 mW/cm^2(circles), 3.1 mW/cm^2(up triangles) and 0.31 mW/cm^2 (down triangles) are indicated in the graph.

modest and reaches approximately 0.01%. It has to be noted that the power efficiencies measured in this work are based on a white light spectrum from a tungsten halogen lamp. Since the solar spectrum has much more weight in the ultraviolet domain than the tungsten lamp and since our devices are more sensitive in the ultraviolet domain, the efficiency values presented here are just a lower estimate.

Quite differently, devices owing mobile counterions have much higher short-circuit currents (Fig. 4b). Clearly, a saturation behavior is observed when the photocurrent density exceeds 10^{-4} A/cm^2. Also the fill factors measured under different light intensities are rather small, and reach 0.16 at an irradiation density of 310 mW/cm^2. Devices made with cyanine films with mobile counterions have power efficiencies that decrease with increasing irradiation intensity from almost 0.09% at 0.31 mW/cm^2 to 0.02% at an irradiation intensity of 310 mW/cm^2.

The reasons for the differences observed between CY10 devices (covalently linked counterions) and CY5 devices (mobile counterions) are not very clear yet. As we will show below, the higher photocurrent in the case of CY5 devices is partly due to the broader spectral photosensitivity of the devices. Furthermore, mobile ions may diffuse from one layer into the other and modify the interfacial energy barriers. Mobile ions are also likely to screen electronic charges and could therefore reduce electron-hole pair recombination while enhancing photocurrent generation.

3.3. Photocurrent spectrum

One of the most striking effects of counterions is manifested in the spectral photocurrent response. The incident photon-to-current conversion efficiency (IPCE) is defined as the number of electrons collected in the external circuit, divided by the number of incident photons per second and is calculated according to

$$\mathrm{IPCE}(\%) = \frac{1240 J_{sc}\,(\mu\mathrm{A/cm^2})}{\lambda(\mathrm{nm})\; P_{in}\,(\mathrm{W/m^2})} \qquad (3)$$

where J_{sc} is the short-circuit photocurrent density generated by the incident monochromatic light with wavelength λ and P_{in} is the incident monochromatic light intensity. Fig. 5a shows the photocurrent spectrum of CY10 devices (with covalently linked counterions) together with the absorption spectrum of the device excluding the aluminum electrode. The fact that the photocurrent maximum at 550 nm corresponds to a minimum of the absorption spectrum (antibatic behavior) indicates that photocurrent generation takes place at the organic interfaces between cyanine and C60. However no current generation is observed in the blue to ultraviolet region of the spectrum, although C60 strongly absorbs at these wavelengths.

Very differently, CY5 based devices exhibit a strong photocurrent response in the blue to UV region. (Fig. 5b). In analogy to other works on C60 based heterojunction photovoltaic devices [14], we have

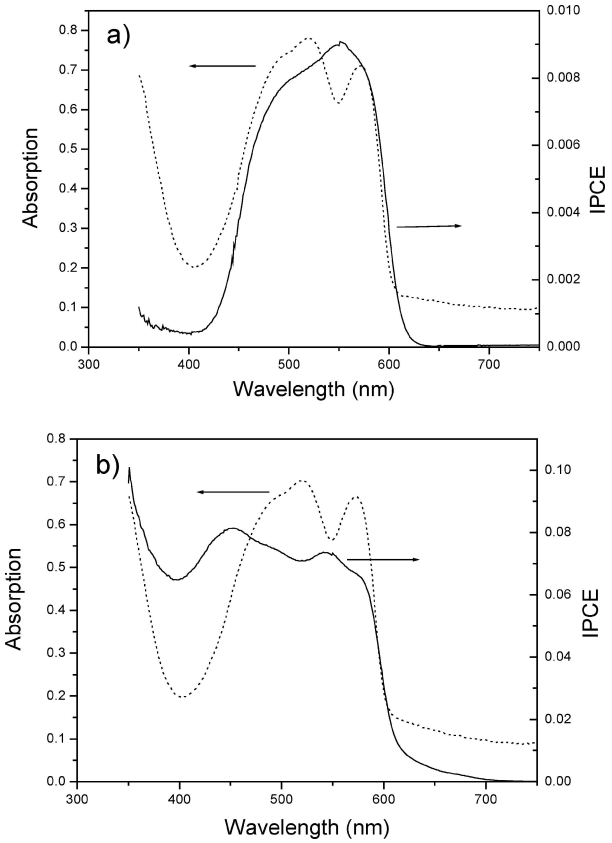

Figure 5 Incident photon to current conversion efficiency (IPCE) spectra at short circuit conditions of devices based on CY10 with covalently linked counterions (a) and devices based on CY5 with free counterions (b). For comparison, the respective absorption spectrum is also indicated in the graph.

attributed this contribution to C60. Certainly the enhanced photo current generation in the blue is responsible for the higher efficiencies measured for this device. This behavior is likely due to the mobile counter ions in CY5. At this stage, it is difficult to precisely elucidate the effect. We believe that the displacement of negative perchlorate ions in the built in filed are responsible. While the electric field in the cyanine layer would be screened, the field across the C60 layer would be enhanced and could give rise to exciton dissociation. Local field effects due to the perchlorate ions inside the C60 layer will also have to be considered.

4. Conclusions

We have investigated counterion effects of cyanine dyes in heterojunction photovoltaic devices. We found that mobile ions are beneficial to device performance. In particular a strong contribution of C60 is observed, which we have attributed to electric field enhancement in the C60 layer. Mobile ions are susceptible to screen charges in the solid film and facilitate charge separation. Ionic dyes such as cyanines could lead the way to ion assisted photoinduced charge separation in solid organic materials.

Acknowledgments

This work is supported by the SNSF (Switzerland) and Shanghai Scientific Committee. We are grateful to Dr. T. Geiger for fruitful discussions.

References

1. N. S. SARICIFTCI, L. SMILOWITZ, A. J. HEEGER and F. WUDL, *Science* **258** (1992) 1474.
2. G. YU, J. GAO, J. C. HUMMELEN, F. WUDL and A. J. HEEGER, *ibid.* **270** (1995) 1789.
3. M. GRANSTROM, K. PETRITSCH, A. C. ARIAS, A. LUX, M. R. ANDERSSON and R. H. FRIEND, *Nature* **395** (1998) 257.
4. S. E. SHAHEEN, C. J. BRABEC, N. S. SARICIFTCI, F. PADINGER, T. FROMHERZ and J. C. HUMMELEN, *Appl. Phys. Lett.* **78** (2001) 841.
5. C. J. BRABEC, S. E. SHAHEEN, C. WINDER, N. S. SARICIFTCI and P. DENK, *ibid.* **80** (2002) 1288.
6. M. SVENSSON, F. L. ZHANG, S. C. VEENSTRA, W. J. H. VERHEES, J. C. HUMMELEN, J. M. KROON, O. INGANAS and M. R. ANDERSSON, *Adv. Mater.* **15** (2003) 988.
7. F. PADINGER, R. S. RITTBERGER and N. S. SARICIFTCI, *Adv. Funct. Mater.* **13** (2003) 85.
8. E. PEETERS, P. A. VAN HAL, J. KNOL, C. J. BRABEC, N. S. SARICIFTCI, J. C. HUMMELEN and R. A. J. JANSSEN, *J. Phys. Chem. B* **104** (2000) 10174.
9. L. SICOT, C. FIORINI, A. LORIN, P. RAIMOND, C. SENTEIN and J. M. NUNZI, *Sol. Energy Mater. Sol. Cells* **63** (2000) 49.
10. J. CABANILLAS-GONZALEZ, S. YEATES and D. D. C. BRADLEY, *Synth. Met.* **139** (2003) 637.
11. T. H. JAMES, "The Theory of the Photographic Process" (Macmillan, Collier Macmillan, New York, London, 1977).
12. F. MENG, K. CHEN, H. TIAN, L. ZUPPIROLI and F. NUESCH, *Appl. Phys. Lett.* **82** (2003) 3788.
13. P. PEUMANS, V. BULOVIC and S. R. FORREST, *ibid.* **76** (2000) 2650.
14. P. PEUMANS and S. R. FORREST, *ibid.* **79** (2001) 126.
15. A. YAKIMOV and S. R. FORREST, *ibid.* **80** (2002) 1667.
16. M. I. DEMCHUK, A. A. ISHCHENKO, V. P. MIKHAILOV and V. I. AVDEEVA, *Chem. Phys. Lett.* **144** (1988) 99.
17. H. NUSBAUMER, S. M. ZAKEERUDDIN, J. E. MOSER and M. GRATZEL, *Chem.-Eur. J.* **9** (2003) 3756.
18. L. A. ERNST, R. K. GUPTA, R. B. MUJUMDAR and A. S. WAGGONER, *Cytometry* **10** (1989) 3.
19. J. WANG, W. F. CAO, J. H. SU, H. TIAN, Y. H. HUANG and Z. R. SUN, *Dyes Pigment.* **57** (2003) 171.
20. R. M. NOYES, *J. Am. Chem. Soc.* **84** (1962) 513.
21. C. ROGERO, J. I. PASCUAL, J. GOMEZ-HERRERO and A. M. BARO, *J. Chem. Phys.* **116** (2002) 832.
22. A. PETR, F. ZHANG, H. PEISERT, M. KNUPFER and L. DUNSCH, *Chem. Phys. Lett.* **385** (2004) 140.
23. Q. B. PEI, .G. YU, C. ZHANG, Y. YANG and A. J. HEEGER, *Science* **269** (1995) 1086.